Review Article

Advances in Bioengineering & Biomedical Science Research

Whole Eye Optical Coherence Tomography Imaging

Cuixia Dai[1], Chunfeng Guo[1], Jiangxue Han[1], Ruiming Kong[1], Wenlu Liu[2], Chuanqing Zhou[2] and Xinyu Chai[2*]

[1]*School of Science, Shanghai Institute of technology, Shanghai, China*

[2]*School of Biomedical Engineering, Shanghai Jiaotong University, Shanghai, China*

[*]Corresponding author

Xinyu Chai, School of Biomedical Engineering, Shanghai Jiaotong University, Shanghai, China, E-mail: xychai@sjtu.edu.cn

Submitted: 12 June 2018; **Accepted**: 19 June 2018; **Published**: 19 July 2018

Abstract

Many eye diseases will affect the shape and dimensions of the whole eye. For examination of ocular accommodation and pathological changes caused by these diseases, high resolution imaging of the whole eye segments OCT system is needed. However, limited by the imaging depth, traditional Fourier Domain Optical Coherence Tomography (FD-OCT) can't be used for real time whole eye segment imaging. In recent years, techniques for depth extended FD-OCT system especially for whole eye segment imaging has been developed. Application on eye parameters measurement and eye accommodation studies were successfully performed. In this paper, both of whole eye FD-OCT techniques and their application were reviewed. Potential clinical application of these techniques may be in the detection of the pathological changes of the whole eye, and whole eye segment FD-OCT system also provides a powerful imaging method for ophthalmic research, such as accommodation, ocular growth, and biometry of the eye.

Introduction

For detection of ocular pathological changes caused by eye diseases like myopia, presbyopia, and glaucoma, high resolution imaging of the whole eye segments is essential for clinical examination. Current technologies applied for whole eye imaging, such as ultrasound imaging and magnetic resonance imaging (MRI) have their advantages and limitations [1-4]. The advantage of ultrasound is its long imaging depth whereas it is a contact imaging technique and its contrast mechanism and resolution are not suitable for imaging the retina [1,2]. High resolution MRI can be applied for whole eye imaging, but it is too costly to be used routinely while its resolution is not high enough to image the retinal layers [3,4].

Optical coherence tomography (OCT) is a noninvasive imaging technology that provides high resolution cross-sectional imaging of biological tissues [5,6]. In recent years, OCT has been becoming an indispensable diagnostic tool in ophthalmology for imaging the retina and anterior segment of the eye. However, limited by the imaging speed of Time-domain OCT (TD-OCT) and imaging depth of traditional Fourier-domain OCT (FD-OCT), effective clinical OCT system for whole eye segment imaging is demanded.

Limitations of Traditional Ophthalmologic OCT Imaging

Since 1991, two types of OCT technique have been investigated, e.g., TD-OCT and FD-OCT. The first OCT system was made in time-domain style, and nowadays some traditional commercial OCT system are still based on TD-OCT, e.g., Visante OCT (Carl Zeiss Meditec) and SL-OCT (Heidelberg Engineering) [5,6]. In TD-OCT, axial ranging (A-scan) is achieved by mechanically scanning the optical path-length delay in the reference arm while continuously recording the low-coherence interference signals. It can be used to image sufficient depth even to cover the full depth of the anterior segment of the eye. However, because of the mechanical scanning used, the imaging speed of these systems is only limited to several kHz A-scan rate. At this imaging speed, inevitable eye movement will limit the accuracy of imaging results.

Currently, FD-OCT takes place of TD-OCT for its high speed and high sensitivity. There are two different FD-OCT system configurations, e.g., Spectral-domain OCT (SD-OCT) and Swept-source OCT (SS-OCT) [7-9]. SD-OCT employs a broadband low-coherence light source while the individual spectral components of the interferogram are detected in parallel by a fast linescan camera in the spectrometer. In contrast, SS-OCT employs an ultrafast sweeping tunable laser while the individual spectral components are detected sequentially by ultrafast photodetectors [10]. However, for deep tissue detection, the imaging depth of FD-OCT is limited by the spectral resolution. In SD-OCT, the spectral resolution is mainly limited by the finite dimension of the pixel detectors in the linescan camera, while instantaneous linewidth of the swept source limits resolution in SS-OCT. Demanded by clinic application of whole eye segment FD-OCT imaging, depth extension techniques should be investigated.

OCT Techniques for Whole Eye Segment Imaging

For whole eye segment imaging, several full-range and combination-image techniques were developed for imaging depth extension in SD-OCT and high quality swept light source were investigated in SS-OCT [11-24].

SD-OCT for Whole Eye Imaging

In SD-OCT system, the imaging depth is restricted by the Hermitian symmetry of Fourier transformation of the real-valued spectral interferogram and the intrinsic limitation of spectral resolution of the

spectrometer [25,26]. Efforts have been made to extend the ranging capability by improving the spectral resolution of the spectrometer in the case of SD-OCT, adding detecting depths of two OCT systems with the two channel arrangement, and using full range complex (FRC) technique to image in the full complex space [11,25,27-34].

However, full-range technique in SD-OCT can not extend imaging depth to whole eye length. In recent years, interlaced detection for anterior segment and retina were proposed and the whole eye segment image was thus constructed [35-42]. In 2012, we presented a dual focus dual channel SD-OCT for simultaneous imaging of the whole eye segments from cornea to the retina [35]. As shown in Figure 1, by using dual channels the system solved the problem of limited imaging depth of SD-OCT and dual focus of the system solved the problem of simultaneous light focusing on the anterior segment of the eye and the retina. In this system, full range complex (FRC) SD-OCT was used in one channel to increase the depth range for anterior segment imaging. The system was successfully tested by imaging a human eye *in vivo*.

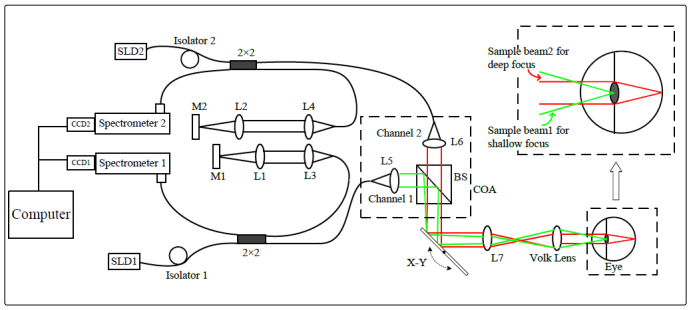

Figure 1: Schematic of the dual focus dual channel OCT experimental system for whole-eye-segment imaging. L1-L7: Lens, M1-M2: Mirror, BS: Beam splitter, COA: Collimating optical assembly [35]

In 2015, we rebuilt the dual focus dual channel OCT with two different bands centered at 840 nm and 1050 nm, which were designed to image the retina and the anterior segments of the eye, respectively, as shown in Figure 2 [38]. By combing the two probe light beams for co-axial scanning and separating them for focusing at different segments of the eye with a combination of three dichroic mirrors, the loss of the backscattered light from the sample was minimized and the imaging depth, scan range and resolution were simultaneously improved. Capability of measuring the dynamic changes of ocular dimensions during accommodation was demonstrated, as shown in Table 1 [37-39].

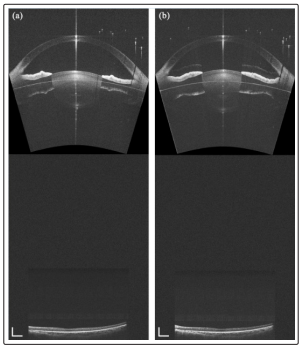

Figure 2: OCT imaging of dynamical change in the whole eye segment from relaxed state (a) to + 6 D accommodated state (b). The frame rate of the movie is 11 fps (approximately 85 ms/frame). Image size: 36.71 mm (depth) × 14 mm (width). White bar: 1 mm [38]

Table 1: The ocular biometry (mean ± standard deviation [SD]) of the whole eye at relaxed and + 6 D accommodated states [38]

Ocular dimensions	Relaxed state	+ 6 D accommodated	Difference	*P*-value[a]
CT (mm)	0.519±0.026	0.518 ± 0.025	-0.001 ± 0.008	0.565
RAC (mm)	7.417±0.243	7.410 ± 0.228	-0.007 ± 0.052	0.661
RPC (mm)	6.264±0.026	6.254 ± 0.200	-0.010 ± 0.064	0.595
EAC	0.519±0.026	0.478 ± 0.055	0.007 ± 0.018	0.207
EPC	0.785±0.055	0.781 ± 0.052	-0.004 ± 0.014	0.331
ACD (mm)	3.646±0.373	3.478 ± 0.365	-0.168 ± 0.015	<0.001
LT (mm)	3.785±0.286	4.059 ± 0.278	0.274 ± 0.021	<0.001
RAL (mm)	10.587±0.503	6.399 ± 0.173	-4.188 ± 0.460	<0.001
RPL (mm)	-6.110 ± 0.185	-4.872 ± 0.191	1.238 ± 0.234	<0.001
EAL	0.960 ± 0.014	0.987 ± 0.013	0.027 ± 0.006	<0.001
EPL	0.950 ± 0.017	0.955 ± 0.016	0.005 ± 0.003	<0.001
VT (mm)	16.917 ± 0.861	16.851 ± 0.857	-0.066 ± 0.016	<0.001
RT (mm)	0.270 ± 0.041	0.256 ± 0.040	-0.014 ± 0.002	<0.001
AL (mm)	24.600 ± 0.955	24.627 ± 0.954	0.027 ± 0.008	<0.001

CT: corneal thickness; RAC and RPC: curvature radius of anterior and posterior corneal surfaces; EAC and EPC: eccentricity of anterior and posterior corneal surfaces; ACD: anterior chamber depth; LT: lens thickness; RAL and RPL: curvature radius of anterior and posterior lens surfaces; EAL and EPL: eccentricity of anterior and posterior lens surfaces; VT: vitreous thickness; RT: retinal thickness; AL: axial length
Difference = + 6 D accommodated - Relaxed

[a]: Paired *t-test*

Other teams were also interested in the whole eye segment SD-OCT imaging. HW Jeong, et al. presented SD-OCT using a single spectrometer with dual illumination and interlaced detection at 830 nm, which can provide anterior segment and retinal tomograms simultaneously, as shown in Figure 3 [40]. Two orthogonal polarization components were used so that both parallel and focused beams could simultaneously be made incident on the eye. This configuration with a polarization-separated sample arm enables us to acquire images from the anterior segment and retina effectively with minimum loss of sample information. However, in the detector arm, a single spectrometer is illuminated via an optical switch for interlaced detection; the anterior segment and the posterior segment are not imaged simultaneously.

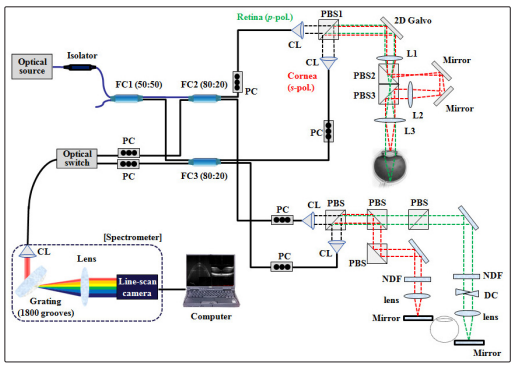

Figure 3: Schematic of dual imaging SD-OCT system at 830 nm designed to acquire *in vivo* images of the anterior segment and the

retina of the eye simultaneously. FC: fiber coupler, PC: polarization controller, CL: collimation lens, PBS: polarization beam splitter, NDF: neutral density filter, DC: dispersion compensation unit, L1-L3: lens [40]

M Ruggeri, et al. and JH Wang, et al. studied on the whole segment imaging by using optical switch to image the corneal epithelium, limbus, ocular surface, contact lens, crystalline lens, retina, and combined the images to be a whole eye segment image [41,42]. The system is based on a single spectrometer and an alternating reference arm with mirrors. Eye parameters and eye accommodation can be detected using their system, as shown in Figure 4. However, due to the refractive power of the anterior segment a light beam can not be focused on both the anterior segment and the retina simultaneously, high lateral resolution whole eye segments images can not be obtained.

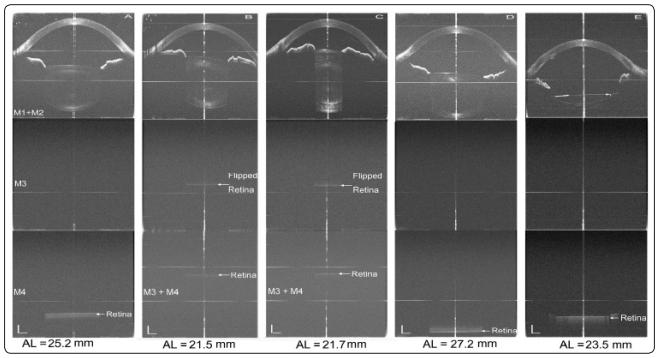

Figure 4: Full eye imaging in different refractive error subjects. (A): Emmetrope; (B) and (C): Hyperope; (D): Myope; (E): Subject with an intraocular lens (IOL). The transverse line artifacts were observed in these images, and the sources of these artifacts may be due to the parasitic reflection in the system. Note the normally oriented retina in (B) and (C) was visible in the combined images obtained with the Mirror 3 and 4 positions. The flipped retina was also visible in the image of the Mirror 3 position due to placement of the zero-delay line inside the eye (bottom of the image). M1-4: refractive mirror position; AL: Axial length. Bars = 1 mm in air [42]

Nowadays, extended-depth SD-OCT for whole eye segment imaging is widely used in eye parameter detecting and examination of ocular accommodation [43-45].

SS-OCT for Whole Eye Imaging

The important light source parameters for SS-OCT include: rapid sweep repetition rates over a wide frequency/wavelength range, single longitudinal mode operation for long coherence length, low excess noise and adjustable laser operation parameters.

A semiconductor laser with a galvanometer tuned grating external cavity at 10 Hz rate was used in SS-OCT early in 1997 [45]. Dramatic increases in speed were achieved using external cavity tunable lasers [46-49]. Currently, external cavity tunable lasers achieve up to a few hundreds of kHz and limitations of relatively long resonators and slow sweep rate are overcome using Fourier-domain mode locking (FDML), which can achieve ultrahigh sweep rates of up to 5.2 MHz by buffering or multiplexing the sweeps [50,51]. Recently, external cavity tunable lasers have been miniaturized using microelectromechanical systems (MEMS) technology [52]. This leads to an increase in sweep rates enabling OCT imaging up to 150 kHz axial scan rates. By using vertical-cavity surface emitting laser (VCSEL) technology, reduction of laser cavity length to achieve single longitudinal mode operation significantly improves SS-OCT performance [53,54].

In 2012, James G Fujimoto reported the full eye imaging by using a SS-OCT system with a VCSEL light source. Imaging was performed on a normal subject with myopia (−7D) [24]. Figure 5 (a) shows a rendering of the full eye from the cornea to the retina. Figure 5 (b) shows a selected cross-sectional image spanning the entire eye from anterior chamber and crystalline lens to the retina. The depth profile in Figure 5 (c) is an averaged axial scan from the central 100 axial scans (central 10 × 10 axial scans). This enables measurement of intraocular distances after correcting for the refractive index of each ocular component. The intensity peaks in Figure 5 (c) can be identified as reflections from the anterior and posterior surfaces of the cornea, anterior and posterior interfaces of the crystalline lens, and retina. The intraocular distances measured using this OCT prototype instrument is shown in Table 2.

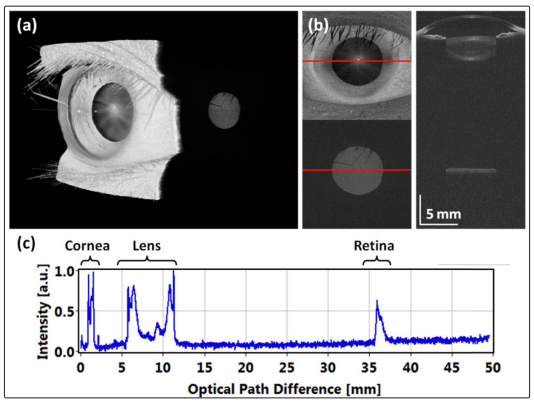

Figure 5: Full eye imaging with ultralong depth range OCT: (a) 3D rendering of volumetric data set, (b) central cross-sectional image and central B-scan extracted from data set corrected for light refraction, (c) central depth profile with echoes from the cornea, crystalline lens and the retina allows for determination of intraocular distances [24]

Table 2: Ocular biometry measurements using VCSEL-OCT [24]

Biometric parameter	VCSEL-OCT
Central corneal thickness	0.52mm
Anterior chamber depth	3.70mm
Lens thickness	3.88mm
Axial eye length	25.77mm

However, due to the refractive power of the anterior segment a light beam can not be focused on both the anterior segment and the retina simultaneously. As seen from the Figure 5, the retina is imaged to be a flat line with bad lateral resolution. This is one of the major reasons why high lateral resolution whole eye segments images can not be obtained using this VCSEL-SS-OCT.

By using coherence revival-based heterodyne SS-OCT, Joseph A Izatt, et al. imaged the anterior and posterior eye simultaneously with high resolution [20]. As shown in Figure 6, a polarization-encoded sample arm was used to efficiently focus orthogonal polarizations on the anterior segment and retina. Depth encoding was achieved

using coherence revival, which allows for multiple depths within a sample to be simultaneously imaged and frequency encoded by carefully controlling the optical path length of each sample path. Results shown in Figure 7, Figure 7A shows a typical B scan as observed during acquisition. Figures 7B and 7C show images from the same data set after further processing, which was averaged over 5 frames. This design is a step towards whole-eye OCT, the realization of which would enable customized ray-traced modeling of patient eyes.

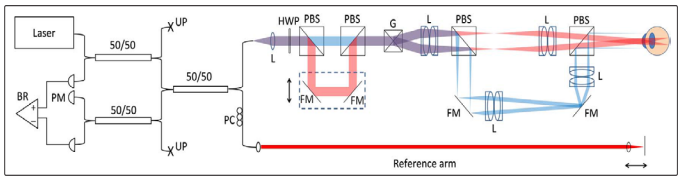

Figure 6: (Color online) SS-OCT system schematic. BR; balanced receiver; PM, power meter; UP, unused ports; PC, polarization controller. Sample arm: red and blue lines depict the retinal and anterior segment imaging paths, respectively. Overlapping paths are shown in purple. L, lens; HWP, half-wave plate; PBS, polarizing beam splitter; FM, fold mirror; G, galvanometers [20]

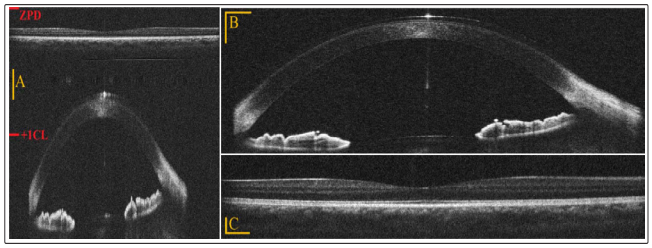

Figure 7: (Color online) Simultaneously acquired anterior segment and retinal images. A, single frame as acquired before cropping, consisting of 2000(lateral) × 2304(axial) samples, acquired in 20 ms. ZPD, zero path length difference position;+1 CL, cavity length offset position. B and C, separated anterior segment and retinal images, averaged over 5 frames. Scale bars are 1 mm, 1 mm × 1 mm, and 250 μm×1° in A, B, and C, respectively. The dynamic ranges of the image data in B and C were 56 and 40 dB, respectively [20]

Take advantage of the long coherence length of swept source and the dual focus dual channel design, high resolution OCT imaging of whole eye segment will be effectively performed.

Discussion and Conclusion

OCT has been rapidly developed for ophthalmic imaging since it was invented 26 years ago. The axial resolution, scan speed, and scan depth are greatly improved. However, since the depth range is determined by the spectrometer design or the instantaneous linewidth of the swept source, traditional FD-OCT are limited to image depth of only a few millimeters. Currently, clinic detection of whole eye pathological changes caused by diseases and examination of ocular accommodation demand high resolution imaging of the whole eye segments OCT system.

Imaging the full human eye depth is a challenge for traditional FD-OCT since the range of the eye structure approximates 24 mm. Therefore, to achieve an extended scan depth to a whole eye depth, some special techniques, including complex conjugate image removal, optical switching, and dual band dual focus have been proposed in SD-OCT. In SS-OCT system, swept light sources of rapid sweep repetition rates over a wide wavelength range, single longitudinal mode operation for long coherence length, low excess noise and adjustable laser operation parameters were presented. Among these techniques, dual band dual focus SD-OCT system and coherence revival-based heterodyne SS-OCT realize the high lateral resolution detection of anterior segment and retina, conquering the limited focus of long-scan-depth FD-OCT. However, the coherence revival-based heterodyne SS-OCT can not image the whole eye depth since its limitation of anterior segment imaging. Nowadays, only dual focus dual channel system can realize the simultaneously imaging the whole eye segment depth with high resolution. Currently, taking advantage of the long coherence length of swept source and the dual focus dual channel design will be a proper choice for whole eye segment high resolution imaging.

In this paper, whole eye FD-OCT techniques and the applications are presented. Whole eye FD-OCT systems provide powerful imaging methods for ophthalmic research, such as accommodation, ocular growth, and biometry of the eye, and potential clinical application of these techniques may be in the detection of the pathological changes of the whole eye.

Acknowledgments

The research is supported by the following grants: National Natural Science Foundation of China (61675134, 61307015), State Key Laboratory of Transient Optics and Photonics, Chinese Academy of Sciences (SKLST201501), Key Research Program, Shanghai Commission for Science and Technology (17441902900), Shanghai Jiao Tong University Interdisciplinary Research Grant on Medicine and Engineering (YG2016ZD07).

References

1. HC Fledelius (1997) Ultrasound in ophthalmology [J]. Ultrasound in Medicine & Biology 23: 365-375.
2. M Restori (2008) Imaging the vitreous: optical coherence tomography and ultrasound imaging [J]. Eye 22: 1251-1256.
3. JE Koretz, SA Strenk, LM Strenk, JL Semmlow (2004) Scheimpflug and high-resolution magnetic resonance imaging of the anterior segment: a comparative study [J]. Journal of the Optical Society of America 21: 346-354.
4. JS Wolffsohn, LN Davies (2007) Advances in anterior segment imaging [J]. Current Opinion in Ophthalmology 18: 32-38.
5. D Huang, EA Swanson, CP Lin, JS Schuman, WG Stinson, et al. (1991) Optical coherence tomography [J]. Science 254: 1178-1181.
6. AF Fercher, W Drexler, CK Hitzenberger, T Lasser (2003) Optical coherence tomography-principles and applications [J]. Reports on Progress in Physics 66: 239-303.
7. RA Leitgeb, CK Hitzenberger, AF Fercher (2003) Performance of Fourier Domain vs. Time Domain optical coherence tomography [J]. Optics Express 11: 889-894.
8. JF de Boer, B Cense, BH Park, MC Pierce, GJ Tearney, et al. (2003) Improved signal to noise ratio in spectral domain compared with time domain optical coherence tomography [J]. Optics Letters 28: 2067-2069.
9. AC Walsh (2011) Binocular optical coherence tomography [J]. Ophthalmic Surgery Lasers & Imaging 42: S95-S105.
10. P Li, L An, GP Lan, M Johnstone, D Malchow, et al. (2013) Extended imaging depth to 12 mm for 1050-nm spectral domain optical coherence tomography for imaging the whole anterior segment of the human eye at 120-kHz A-scan rate [J]. Journal

of Biomedical Optics 18: 016012-1- 016012-4.
11. CQ Zhou, JH Wang, SL Jiao (2009) Dual channel dual focus optical coherence tomography for imaging accommodation of the eye [J]. Optics Express 17: 8947- 8955.
12. AF Fercher, R Leitgeb, CK Hitzenberger, H Sattmann, M Wojtkowski (1999) Complex spectral interferometry OCT [C]. Proc. SPIE 3564: 173-178.
13. M Wojtkowski, A Kowalczyk, R Leitgeb, A Fercher (2002) Full range complex spectral optical coherence tomography technique in eye imaging [J]. Optics Letters 27: 1415-1417.
14. RA Leitgeb, CK Hitzenberger, AF Fercher, T Bajraszewski (2003) Phase shifting algorithm to achieve high-speed long-depth-range probing by frequency-domain optical coherence tomography [J]. Optics Letters 28: 2201-2203.
15. E Götzinger, M Pircher, R Leitgeb, CK Hitzenberger (2005) High speed full range complex spectral domain optical coherence tomography [J]. Optics Express 13: 583-594.
16. B Baumann, M Pircher, E Götzinger, CK Hitzenberger (2007) Full range complex spectral domain optical coherence tomography without additional phase shifters [J]. Optics Express 15: 13375-13387.
17. L An, R Wang (2007) Use of a scanner to modulate spatial interferograms for *in vivo* full-range Fourier-domain optical coherence tomography [J]. Optics Letters 32: 3423-3425.
18. R Leitgeb, R Michaely, T Lasser, S Sekhar (2007) Complex ambiguity-free Fourier domain optical coherence tomography through transverse scanning [J]. Optics Letters 32: 3453-3455.
19. J Jungwirth, B Baumann, M Pircher, E Gotainger, CK Hitzenberger (2009) Extended *in vivo* anterior eye-segment imaging with full-range complex spectral domain optical coherence tomography [J]. Journal of Biomedical Optics 14: 050501.
20. AH Dhalla, D Nankivil, T Bustamante, A Kuo, JA Izatt (2013) Simultaneous swept source optical coherence tomography of the anterior segment and retina using coherence revival [J]. Optics Letters 37: 1883-1885.
21. H Furukawa, H Hiro-Oka, N Satoh, R Yoshimura, D Choi, et al. (2010) Full-range imaging of eye accommodation by high-speed long-depth range optical frequency domain imaging [J]. Biomedical Optics Express 1: 1491-1501.
22. M Gora, K Karnowski, M Szkulmowski, BJ Kaluzny, R Huber, et al. (2009) Ultra high-speed swept source OCT imaging of the anterior segment of human eye at 200 kHz with adjustable imaging range [J]. Optics Express 17: 14880-14894.
23. B Potsaid, B Baumann, D Huang, S Barry, AE Cable, et al. (2010) Ultrahigh speed 1050nm swept source/Fourier domain OCT retinal and anterior segment imaging at 100,000 to 400,000 axial scans per second [J]. Optics Express 18: 20029-20048.
24. I Grulkowski, JJ Liu, B Potsaid, V Jayaraman, CD Lu, et al. (2012) Retinal, anterior segment and full eye imaging using ultrahigh speed swept source OCT with verticalcavity surface emitting lasers [J]. Biomedical Optics Express 3: 2733-2751.
25. AF Fercher, CK Hitzenberger, G Kamp, SY El-Zaiat (1995) Measurement of intraocular distances by backscattering spectral interferometry [J]. Optics Communications 117: 43-48.
26. G Häusler, MW Lindner (1998) Coherence radarand spectralradar-new tools for dermatological diagnosis [J]. Journal of Biomedical Optics 3: 21-31.
27. AF Fercher, R Leitgeb, CK Hitzenberger, H Sattmann, M Wojtkowski (1999) Complex spectral interferometry OCT [C]. Proc. SPIE 3564: 173-178.
28. M Wojtkowski, A Kowalczyk, R Leitgeb, A Fercher (2002) Fullrange complex spectral optical coherence tomography technique in eye imaging [J]. Optics Letters 27: 1415-1417.
29. RA Leitgeb, CK Hitzenberger, AF Fercher, T Bajraszewski (2003) Phaseshifting algorithm to achieve high-speed long-depth-rangeprobing by frequency-domain optical coherence tomography [J]. Optics Letters 28: 2201-2203.
30. E Götzinger, M Pircher, R Leitgeb, CK Hitzenberger (2005) Highspeed full range complex spectral domain optical coherence tomography [J]. Opt. Express 13: 583-594.
31. B Baumann, M Pircher, E Götzinger, CK Hitzenberger (2007) Full range complex spectral domain optical coherence tomography without additional phase shifters [J]. Opt. Express 15: 13375-13387.
32. L An, R Wang (2007) Use of a scanner to modulate spatial interferograms for *in vivo* full-range Fourier-domain optical coherence tomography [J]. Optics Letters 32: 3423-3425.
33. R Leitgeb, R Michaely, T Lasser, S Sekhar (2007) Complex ambiguity-free Fourier domain optical coherence tomography through transverse scanning [J]. Optics Letters 32: 3453-3455.
34. J Jungwirth, B Baumann, M Pircher, E Gotainger, CK Hitzenberger (2009) Extended *in vivo* anterior eye-segment imaging with full-range complex spectral domain optical coherence tomography [J]. Journal of Biomedical Optics 14: 050501.
35. CX Dai, CQ Zhou, SH Fan, Z Chen, XY Chai, et al. (2012) Optical coherent tomography for whole eye segment imaging [J]. Optics Express 20: 6109-6115.
36. SH Fan, Y Sun, CX Dai, CQ Zhou (2014) Accommodation-induced variations in retinal thickness measured by spectral domain optical coherence tomography [J]. Journal of Biomedical Optics 19: 096012-1-096012-8.
37. S Yong, SH Fan, CX Dai, CQ Zhou (2014) Noninvasive imaging and measurement of accommodation using dual-channel SD-OCT [J]. Current eye research 39: 611-619.
38. SH Fan, L Li, Q Li, CX Dai, QS Ren, et al. (2015) Dual band dual focus optical coherence tomography for imaging the whole eye segment [J]. Biomedical Optics Express 6: 2481-2493.
39. SH Fan, Y Sun, CX Dai, CQ Zhou (2014) The Whole Eye Segment Imaging and Measurement with Dual Channel SD-OCT [J]. Ophthalmic Surgery, Lasers and Imaging retina 28: 317-322.
40. HW Jeong, SW Lee, BM Kim (2012) Spectral-domain OCT with dual illumination and interlaced detection for simultaneous anterior segment and retina imaging [J]. Optics Express 20: 19148-19159.
41. M Ruggeri, SR Uhlhorn, C De Freitas, A Ho, F Manns, et al. (2012) Imaging and full-length biometry of the eye during accommodation using spectral domain OCT with an optical switch [J]. Biomedical Optics Express 3: 1506-1520.
42. Zhong J, Tao A, Xu Z, Jiang H, Shao Y, et al. (2014) Whole eye axial biometry during accommodation using ultra-long scan depth optical coherence tomography [J]. American Journal of Ophthalmology 157: 1064-1069.
43. YC Chang, K Liu, CD Freitas, A Pham, F Cabot, et al. (2017) Assessment of eye length changes in accommodation using dynamic extended-depth OCT [J]. Biomedical Optics Express 8: 2709-2719.
44. HJ Kim, PU Kim, MG Hyeon, Y Choi, J Kim, et al. (2016) High-resolution, dual-depth spectral-domain optical coherence tomography with interlaced detection for whole-eye imaging

[J]. Applied Optics 55: 7212-7217.
45. SR Chinn, EA Swanson, JG Fujimoto (1997) Optical coherence tomography using a frequency-tunable optical source [J]. Optics Letters 22: 340-342.
46. SH Yun, C Boudoux, GJ Tearney, BE Bouma (2003) High-speed wavelength-swept semiconductor laser with a polygon-scanner-based wavelength filter [J]. Optics Letters 28: 1981-1983.
47. MA Choma, K Hsu, JA Izatt (2005) Swept source optical coherence tomography using an all-fiber 1300-nm ring laser source [J]. Journal of Biomedical Optics 10: 044009.
48. R Huber, M Wojtkowski, K Taira, JG Fujimoto, K Hsu (2005) Amplified, frequency swept lasers for frequency domain reflectometry and OCT imaging: design and scaling principles [J]. Optics Express 13: 3513-3528.
49. BD Goldberg, SM Motaghian Nezam, P Jillella, BE Bouma, GJ Tearney (2009) Miniature swept source for point of care optical frequency domain imaging [J]. Optics Express 17: 3619-3629.
50. R Huber, M Wojtkowski, JG Fujimoto (2006) Fourier Domain Mode Locking (FDML): A new laser operating regime and applications for optical coherence tomography [J]. Optics Express 14: 3225-3237.
51. W Wieser, BR Biedermann, T Klein, CM Eigenwillig, R Huber (2010) Multi-megahertz OCT: High quality 3D imaging at 20 million A-scans and 4.5 G Voxels per second [J]. Optics Express 18: 14685-14704.
52. AQ Liu, XM Zhang (2007) "A review of MEMS external-cavity tunable lasers," Journal of Micromechanics and Microengineering 17: R1-R13.
53. V Jayaraman, J Jiang, H Li, PJS Heim, GD Cole, et al. (2011) OCT imaging up to 760 kHz axial scan rate using single-mode 1310 nm MEMS-tunable VCSELs with >100 nm tuning range [C], Conference on Lasers and Electro-Optics, Technical Digest (CD), (Optical Society of America) PDPB2.
54. B Potsaid, V Jayaraman, JG Fujimoto, J Jiang, PJS Heim, et al. (2012) MEMS tunable VCSEL light source for ultrahigh speed 60 kHz-1 MHz axial scan rate and long range centimeter class OCT imaging [C], Proc. SPIE 8213: 82130M, 82130M-8.